

$$[k_{21}] = [k_{12}]^T = [0 \quad -k_b] \quad (12b)$$

$$[k_{22}] = [k_b] \quad (12c)$$

$$[m_{11}] = \begin{bmatrix} m_a & 0 \\ 0 & m_b \end{bmatrix} \quad (12d)$$

$$[m_{21}] = [m_{12}]^T = [0 \quad 0] \quad (12e)$$

$$[m_{22}] = [m_c] \quad (12f)$$

$$\{x_1\} = \begin{Bmatrix} y_a \\ y_b \end{Bmatrix} \quad (12g)$$

$$\{x_2\} = \{y_c\} \quad (12h)$$

Consistent with Eq. (3), the rigid-body transformation matrix is given by

$$[T_{12}] = \begin{Bmatrix} 1 \\ 1 \end{Bmatrix} \quad (13)$$

Substitution of Eqs. (12) and (13) into Eqs. (10) gives

$$[R] = -m_c^{-1}[m_a \quad m_b] \quad (13a)$$

$$[K_R] = m_c^{-1} \begin{bmatrix} k_a m_c & -k_a m_c \\ k_b m_a - k_a m_c & (k_a + k_b)m_c + k_b m_b \end{bmatrix} \quad (13b)$$

$$[M_R] = \begin{bmatrix} m_a & 0 \\ 0 & m_b \end{bmatrix} \quad (13c)$$

Therefore, the reduced-system determinantal equation for the two nonzero frequencies becomes

$$D_2 = \begin{vmatrix} k_a - \omega^2 m_a & -k_a \\ k_b(m_a/m_c) - k_a & (k_a + k_b) + k_b(m_b/m_c) - \omega^2 m_b \end{vmatrix} = 0 \quad (14)$$

It is easily shown that the characteristic equation for the same problem when attacked in the unreduced conventional manner is given by $\omega^2 D_2 = 0$, which has the rigid-body zero frequency as one additional solution.

Symmetrical Form of the Reduced System Equations

Since many algorithms for extracting eigenvalues require that the stiffness and mass matrices be symmetric, an alternative formulation of Eq. (9), leading to symmetric reduced stiffness and mass matrices, is presented. Combining Eqs. (2a), (8), and (10c) yields

$$\{x\} = [S]\{x_1\} \quad (15)$$

where

$$[S] = \begin{bmatrix} I_{n-r} \\ R \end{bmatrix} \quad (16)$$

and $[I]_{n-r}$ is an identity matrix with the same order as $[k_{11}]$. Substitution of Eqs. (15) into (1) and premultiplication by $[S]^T$ then yields

$$[\bar{K}_R]\{x_1\} = \omega^2 [\bar{M}_R]\{x_1\}, \omega^2 \neq 0 \quad (17)$$

where

$$[\bar{K}_R] = [S]^T [k] [S] \quad (18a)$$

and

$$[\bar{M}_R] = [S]^T [m] [S] \quad (18b)$$

Thus, the reduced system may be defined by the symmetric matrix Eq. (17), or the unsymmetric matrix Eq. (9).

Appendix

The rigid-body transformation matrix $[T_{12}]$ can also be expressed in terms of the stiffness matrix partitions by noting that

$$\begin{bmatrix} k_{11} & k_{12} \\ k_{21} & k_{22} \end{bmatrix} \begin{Bmatrix} x_1 \\ x_2 \end{Bmatrix}_0 = \{0\}$$

from which $\{x_1\}_0 = -[k_{11}]^{-1}[k_{12}]\{x_2\}_0$. Comparing this result with Eq. (3) reveals that

$$[T_{12}] = -[k_{11}]^{-1}[k_{12}]$$

From a computational point of view, however, it should be noted that the evaluation of $[T_{12}]$ as above requires inversion of $[k_{11}]$ which, for large, complex structures, is approximately of the same order as the system's assembled stiffness matrix. Therefore, unless $[k_{11}]^{-1}$ is available from previous calculations, $[T_{12}]$ is best generated directly from kinematical considerations.

References

- ¹ Tong, K. N., *Theory of Mechanical Vibration*, Wiley, New York, 1960, pp. 198-202.
- ² Wilkinson, J. H., *The Algebraic Eigenvalue Problem*, Clarendon Press, Oxford, England, 1965.
- ³ Mack, C. E., "Tensor Analysis of Aircraft Structural Vibration," Paper 104, Jan. 1948, IAS.
- ⁴ Rodden, W. P., "On Vibration and Flutter Analysis with Free-Free Boundary Conditions," *Journal of the Aeronautical Sciences*, Vol. 28, Jan. 1961, pp. 65-66.
- ⁵ Berman, J. H. and Sklerov, J., "Calculation of Natural Modes of Vibration for Free-Free Structures in Three-Dimensional Space," *AIAA Journal*, Vol. 3, No. 1, Jan. 1965, pp. 158-160.
- ⁶ Crandall, S. H., *Engineering Analysis*, McGraw-Hill, New York, 1956.

Virtual Origins of a Free Plane Turbulent Jet

JAMES J. FLORA JR.* AND VICTOR W. GOLDSCHMIDT†
Purdue University, Lafayette, Ind.

Nomenclature

- b_a = jet half-width (measured to location where $U/U_m = \frac{1}{2}$)
 C_1 = location of the geometric origin from the slot made dimensionless by d
 C_2 = location of the kinematic origin from the slot made dimensionless by d
 d = slot width
 K_1 = rate of widening of the jet, defined by Eq. (1)
 K_2 = slope of the centerline velocity decay, defined by Eq. (2)
 \bar{U}_m = velocity at the axis of the jet
 \bar{U}_0 = velocity at the mouth of the jet (at $x = 0$)
 x = distance along the axis measured from the mouth of the jet

TWO different origins of similarity in turbulent freejets may be defined. One is based on the widening of the jet, the other on the decay of the axial velocity. Tests (for

Received February 28, 1969; revision received September 15, 1969. The reported work was made possible through an NSF URP Grant GY 6058.

* National Science Foundation Undergraduate Research Participant, School of Civil Engineering.

† Associate Professor, School of Mechanical Engineering.

Table 1 Plane freejet characteristics

Investigator	K_1	C_1	K_2	C_2	Slot size	Plenum chamber	Nozzle shape	Straightener
Foss ⁵	0.0625	-2.00	0.1885	6.5	1.99 in. × 6.00 in.	44 in. × 44 in.	Beam deflection	Eggcrate, screening
Goldschmidt ⁶	0.0985	0.66	0.2068	5.83	0.9 in. × 14.5 in.	21.5 × 14.5	Gradual circular	Honeycomb, cheese-cloth, screening
Heskestad ⁷	0.110	5.3	0.364	5.3	0.50 in. × 66 in.	...	Long channel	...
Householder ⁸	0.0908	-1.46	0.1927	6.98	0.93 in. × 15 in.	13 in. × 15 in.	Gradual	Honeycomb, screening
Miller and Comings ³	0.0723	-1.572	0.167	-1.572	0.50 in. × 20 in.	23.5 in. × 23.5 in.	Gradual circular	Honeycomb, screening
Van der Hegge Zijnen ⁹	0.100	...	0.205	-1.7	1 cm × 25 cm	26 cm tube	Abrupt	...
Van der Hegge Zijnen ⁹	0.095	...	0.162	-0.6	5 cm × 10 cm	4 in. tube	Abrupt	...

Reynolds numbers in the order of 10^4) show the location of these virtual origins to be different from each other, independent of the shape of the contracting section between the plenum chamber and the mouth of the jet, but strongly dependent on the turbulence intensity downstream of the plenum chamber.

The virtual origin of a freejet may be identified in two different ways. For convenience these are defined as the geometric and the kinematic origins, respectively.

Within the zone of established flow the jet widens linearly with x and the velocity at the axis decreases with the $\frac{1}{2}$ power of x . If $(\bar{U}_m/\bar{U}_0)^{-2}$ is plotted against x/d , a straight-line relationship results. The kinematic origin is defined as the (extrapolated) intercept with the abscissa of the resulting straight line. Similarly, the geometric origin is defined by the intersection of the two boundary lines defining the zone of established flow.

What first appears rather paradoxical is that these two virtual origins do not necessarily coincide. They furthermore are located in differing locations for different experimental setups, sometimes upstream and other times downstream of the physical origin of the jet.

Two-dimensional jet flows have been well documented. (For instance, see Abramovich,¹ Albertson,² Miller,³ and Sato.⁴) In general we can formulate

$$b_u/d = K_1 (x/d - C_1) \quad (1)$$

$$(\bar{U}_m/\bar{U}_0)^{-2} = K_2 (x/d - C_2) \quad (2)$$

For low subsonic jets where Mach number effects are negligible the spreading rate, K_1 (and hence also K_2) is ex-


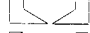
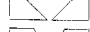
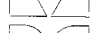
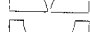





pected to be constant and independent of upstream conditions; on the other hand the values for C_1 and C_2 could well be expected to depend on upstream conditions particularly in the manner of contraction. A review of the results of earlier investigations leads to Table 1. As can be readily seen, there seems to be no pattern to the location of either the geometric or velocity origins.

In an attempt to determine the influence of upstream conditions on the location of the jet origins of similarity two different tests were performed. In the first a series of different contraction nozzle block sections were located upstream of the 0.50 in. × 25.0 in. slot. Sections were cut forming styrofoam blocks into considerably different contours. The experimental setup is shown in Fig. 1. The slot was on a vertical wall which extended 15 in. from either side. The two-dimensional jet in turn was confined between two horizontal plywood sheets extending 50 in. downstream from the orifice and 15 in. to either side of it.

The Reynolds numbers of the flow based on the slot's width ranged from 1.71×10^4 to 2.90×10^4 . Each nozzle was tested at two extreme velocities showing comparable results for the constants C_1 , C_2 , K_1 , and K_2 . All measurements were taken up to 90 slot widths downstream from the slot with a Pitot-static tube and a Meriam Instrument Company model 34FB2 micromanometer. Table 2 tabulates the corresponding results.†

As expected there is not a necessary coincidence of the geometric and kinematic origins. However, what is startling is that changes of the contracting section did not influence the location of these origins nor the widening and decay rates as noted by the essentially constant values of K_1 and K_2 . In all cases shown the plenum chamber had a width of 33.5 in. To ascertain that the relative size of the inlet area of the contraction nozzle was not too small a series of tests were repeated with the plenum chamber width reduced to 10.5 in. The results for all practical purposes remained unchanged.

Table 2 Geometric and kinematic origins for different nozzle shapes

NOZZLE BLOCK SECTION	K_1	C_1	K_2	C_2
	0.111	0	0.160	2.5
	0.113	0	0.163	2.5
	0.113	0	0.165	2.5
	0.111	0	0.159	2.5
	0.108	0	0.164	2.5
	0.112	0	0.161	2.5
	0.112	0	0.164	2.5
	0.111	0	0.161	2.5
	0.109	0	0.158	2.5
	0.109	0	0.162	2.5

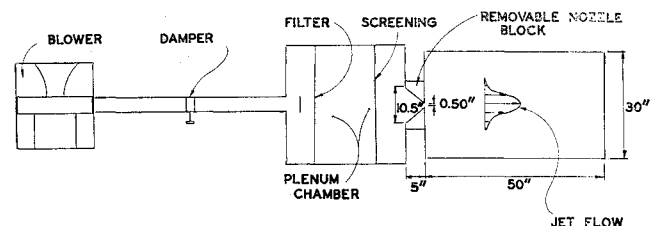


Fig. 1 Schematic of experimental setup.

† The value of U was determined by computing the momentum flux from measured profiles at various x stations. Constancy of momentum was confirmed. This way the erroneous interpretation of measured velocity at the mouth (when the static pressure gradient in the immediate region is not accounted for) was avoided.

Table 3

Setup	Geometric origin		Kinematic origin		Measured turbulence intensity, ^a %		
	K ₁	C ₁	K ₂	C ₂	1	2	3
Screen and filter	0.130	-15.0	0.227	2.00	1.06	0.975	2.81
Filter only	0.127	-5.00	0.222	0	1.28	1.45	3.66
Filter and rods	0.113	-6.00	0.194	-1.00	1.21	1.45	2.82

^a 1 Turbulence at mouth of jet; 2 Turbulence $\frac{1}{2}$ in. upstream from mouth of jet; 3 Turbulence $\frac{1}{4}$ in. upstream from mouth of jet.

Having discarded the possibility that the shape of the contracting nozzle could influence the location of the origins a second test was run to determine whether upstream conditions capable of changing the stream turbulence had a considerable effect.

In this second test, a different 25 in. \times 25 in. plenum chamber was used. The slot was 1 in. wide by 25 in. high. The slot ended in a wall extending 24 in. from either side of it. The resulting two-dimensional jet was confined between two horizontal plywood sheets now extending 96 in. downstream and 24 in. to each side, similar to the earlier test. The Reynolds number of the flow from the orifice based on the slot's width ranged from 2.3×10^4 to 2.55×10^4 . The plenum chamber was similar to that of the first run except for the fact that the wire screening was removable and could be replaced by a series of $\frac{1}{4}$ in. square rods, 2 in. on center. This was purposely done to provide three different configurations giving different turbulence intensities upstream of the slot. The results are shown in Table 3.

In the aforementioned, the obvious observation is that the location of the virtual origins can be drastically changed by affecting plenum chamber conditions. There appears to also be a slight decrease in the widening and decay rates with upstream turbulence. The tabulated measurements of turbulence intensity were crude spot checks taken only at the center of the jet. The configurations suggest that a slight increase of turbulence upstream of the contraction may move the virtual origins considerably upstream. This may be explained by the enhanced mixing. At the same time these appear to be independent of nozzle shape, plenum chamber width and slot width, and what is of even greater interest they do not tend to coincide in their locations. This lack of coincidence in location of the two virtual origins and their seemingly strong dependence on stream turbulence intensity casts a new light into the usual concept of a unique origin of similarity in turbulent freejets.

References

- ¹ Abramovich, G. N., *The Theory of Turbulent Jets*, The M.I.T. Press, Cambridge, Mass., 1963.
- ² Albertson, M. J. et al., "Diffusion of Submerged Jets," *Proceedings of the American Society of Chemical Engineers*, Vol. 74, Dec. 1948, pp. 1571-1596.
- ³ Miller, D. R. and Comings, E. W., "Static Pressure Distribution in the Free Turbulent Jet," *Journal of Fluid Mechanics*, Vol. 3, No. 1, Oct. 1957, pp. 1-16.
- ⁴ Sato, H., "The Stability and Transition of a Two-Dimensional Jet," *Journal of Fluid Mechanics*, Vol. 7, No. 5, 1959, pp. 53-80.
- ⁵ Foss, J. F., "A Study of Incompressible Bounded Turbulent Jets," Ph.D. thesis, Jan. 1965, Purdue Univ.
- ⁶ Goldschmidt, V. W., "Two-Phase Flow in a Two-Dimensional Turbulent Jet," dissertation, Jan. 1965, Syracuse Univ.
- ⁷ Heskestad, G., "Hot-Wire Measurements in a Plane Turbulent Jet," *Transactions of the ASME, Journal of Applied Mechanics*, Dec. 1965, pp. 721-734.
- ⁸ Householder, M. K. and Goldschmidt, V. W., "Turbulent Diffusion of Small Particles in a Two-Dimensional Free Jet," TR FMTR 68-3, 1968, National Science Foundation.
- ⁹ Van der Hegge Zijnen, B. G., "Measurements of the Velocity Distribution in a Plane Turbulent Jet of Air," *Applied Scientific Research*, Vol. 7, Sec. A, 1957, pp. 256-276.

Buckling of Clamped and Simply Supported Shallow Spherical Shells

GERALD A. COHEN*

Structures Research Associates, Newport Beach, Calif.

IN Ref. 1, Stein has compared the theoretical buckling pressures for shallow spherical shells with clamped (Refs. 2 and 3) and simply supported edges (Ref. 3). He states that a paradox exists for $3 < \lambda < 5$, where λ is the usual shallow spherical shell parameter $2[3(1 - \nu^2)]^{1/4}(H/t)^{1/2}$, since in this region the buckling pressure for clamped edges is apparently below that for simply supported edges. He also suggests the possibility that in this region the $N = 1$ buckling mode (which was not studied in Ref. 3) may be critical for simply supported edges, and that the associated critical pressure may be below the clamped shell buckling pressure.

These statements are no doubt based on the assumption that the introduction of additional edge constraint increases the buckling load, which, of course, is the case for most structures. This assumption is, in fact, based on the energy method of solution, in which the buckling load is usually expressed as the minimum value of a certain functional of kinematically admissible displacement fields. Since the introduction of additional edge constraint reduces the family of admissible displacements, it also must raise (at least, not lower) the associated minimum value, i.e., the buckling load. However, it is frequently overlooked that this functional, by virtue of its dependence on the prebuckling state, also changes with the introduction of additional edge constraint. Insofar as this occurs, the aforementioned argument breaks down and additional edge constraint can, in fact, reduce the buckling load (as indeed it does when a shallow segment is cut from a complete spherical shell and its edges are clamped). Therefore, no paradox really exists. On the other hand, the $N = 1$ mode should be investigated for simply supported edges, and to assess its importance a brief study, using computer programs based on the analyses presented in Refs. 4 and 5, was made and is reported here.

For this purpose, a 20° spherical cap with $t/R = 0.02462$ and $\nu = \frac{1}{3}$, corresponding to $\lambda = 4$, loaded by a uniform normal pressure field was considered. For this shell, the classical buckling pressure p_{cl} is given by $p_{cl}/E \times 10^5 = 74.24$. The dimensionless prebuckling stiffness KR^3/E and its derivative with respect to the dimensionless pressure p/E were computed for four values of p/p_{cl} for simply supported edges and two values of p/p_{cl} for clamped edges. These results are shown in Table 1. The results given in Table 1 are plotted in Fig. 1, in which the curves have been extrapolated to zero stiffness, corresponding to the limit load pressure p_0 . As shown, for clamped edges $p_0/p_{cl} = 0.583$, which agrees well with the value 0.578 given in Ref. 2. As expected from the results of Ref. 3, removing the rotational edge constraint increases the limit load. The value obtained, $p_0/p_{cl} = 0.710$, is, however, significantly greater than the value 0.65 given in Ref. 3.

Table 1 Stiffness variation of shallow spherical shells ($\lambda = 4$)

p/p_{cl}	$p/E \times 10^5$	Simply supported		Clamped	
		KR^3/E	$d(KR^3)/dp$	KR^3/E	$d(KR^3)/dp$
0.5	37.12	0.1212	-374	0.1323	-896
0.578	42.91	0.0372	-4404
0.6	44.54	0.0897	-495
0.65	48.26	0.0684	-698
0.7	51.97	0.0258	-2247

Received June 9, 1969; revision received August 19, 1969.

* President and Technical Director. Member AIAA.